

THE STELLAR MASS TULLY-FISHER RELATION TO $Z = 1.2$ FROM AEGIS

SUSAN A. KASSIN¹, BENJAMIN J. WEINER², S. M. FABER¹, DAVID C. KOO¹, JENNIFER M. LOTZ³, JÜRG DIEMAND^{1,4}, JUSTIN J. HARKER¹, KEVIN BUNDY⁵, A. J. METEVIER¹, ANDREW C. PHILLIPS¹, MICHAEL C. COOPER⁶, DARREN J. CROTON⁵, NICHOLAS KONIDARIS¹, KAI G. NOESKE¹, & C. N. A. WILLMER^{2,7}

Accepted for Publication in the ApJL

ABSTRACT

We combine newly measured rotation velocities, velocity dispersions, and stellar masses to construct stellar mass Tully-Fisher relations (M_* TFRs) for 544 galaxies with strong emission lines at $0.1 < z < 1.2$ from the All Wavelength Extended Groth Strip International Survey (AEGIS) and the Deep Extragalactic Evolutionary Probe 2 Survey (DEEP2). The conventional M_* TFR using only rotation velocity (V_{rot}) shows large scatter (~ 1.5 dex in velocity). The scatter and residuals are correlated with morphology in the sense that disturbed, compact, and major merger galaxies have lower velocities for their masses. We construct an M_* TFR using the kinematic estimator $S_{0.5}$ which is defined as $\sqrt{0.5V_{rot}^2 + \sigma_g^2}$ and accounts for disordered or non-circular motions through the gas velocity dispersion (σ_g). The new M_* TFR, termed $S_{0.5}/M_*$ TFR, is remarkably tight over $0.1 < z < 1.2$ with no detectable evolution of its intercept or slope with redshift. The average best fit relation has 0.47 dex scatter in stellar mass, corresponding to ~ 1.2 ‘magnitudes,’ assuming a constant mass-to-light ratio. Interestingly, the $S_{0.5}/M_*$ TFR is consistent with the absorption-line based stellar mass Faber-Jackson relation for nearby elliptical galaxies in terms of slope and intercept, which might suggest a physical connection between the two relations.

Subject headings: galaxies: evolution – galaxies: general – galaxies: high-redshift – galaxies: interactions – galaxies: kinematics and dynamics – galaxies: spiral

1. INTRODUCTION

The Tully-Fisher relation (TFR) between the luminosity of galaxies and their rotation velocity is a fundamental scaling relation that constrains galaxy formation and evolution models (e.g., Dalcanton, Spergel, & Summers 1997, and references therein). Recent local studies focus on stellar or baryonic masses (e.g., Bell & de Jong 2001; McGaugh 2005; Pizagno et al. 2005), which are easier to model than luminosity. Distant stellar-mass TFRs (M_* TFRs) have also been studied (Conselice et al. 2005; Flores et al. 2006). Neither found evidence for evolution to redshifts $z \sim 1$ or 0.6, respectively, but each pruned their data to exclude morphologically odd galaxies. This letter presents a study of the M_* TFR to redshift $z = 1.2$ using a sample of 544 galaxies with strong emission lines. Following Weiner et al. (2006b), we exclude few galaxies and adopt a new velocity measure that includes both velocity gradients (usually rotation) and velocity spread (dispersion). We adopt a Λ CDM cosmology with $h = 0.7$, $\Omega_m = 0.3$, and $\Omega_\Lambda = 0.7$.

2. OBSERVATIONS

¹ UCO/Lick Observatory, Department of Astronomy & Astrophysics, University of California, Santa Cruz, CA 95064; kassin, faber, koo, jharker, anne, phillips, npk, kai, and diemand@ucolick.org

² Steward Observatory, University of Arizona, Tucson, AZ; bjw@as.arizona.edu, cnaw@as.arizona.edu

³ Leo Goldberg Fellow, National Optical Astronomical Observatories, Tucson, AZ; lotz@noao.edu

⁴ Hubble Fellow

⁵ Reinhardt Fellow, University of Toronto, Toronto, Canada; bundy@astro.utoronto.ca

⁶ Department of Astronomy, University of California, Berkeley, CA; cooper@astron.berkeley.edu, darren@astron.berkeley.edu

⁷ On leave from Observatório Nacional, Brazil.

Galaxy kinematics and morphologies at $z \sim 1$ are possible with high resolution spectra and images. To track different morphologies and redshifts, samples should be large enough to be subdivided. The All-Wavelength Extended Groth Strip International Survey (AEGIS) provides such data. Single-orbit images were taken by the Hubble Space Telescope Advanced Camera for Surveys (HST/ACS) in the F606W (V) and F814W (I) bandpasses, and spectra were obtained by the Deep Extragalactic Evolutionary Probe 2 Survey (DEEP2); see details in Davis et al. (2003, 2006). Observations and reduction of kinematics are described in Weiner et al. (2006a) for data similar to DEEP2. Kinematics are measured from the strongest emission line(s) among $H\alpha$, $H\beta$, $[OII] \lambda 3727$, and $[O III] \lambda 5007$. The spectral resolution is $FWHM = 1.4 \text{ \AA}$, or 56 km s^{-1} at $z = 1$ (Gaussian $\sigma = 24 \text{ km s}^{-1}$). Emission line widths can be measured down to ~ 0.6 of the σ or $\sim 15 \text{ km s}^{-1}$, and velocity centroids for rotation curves are good to 0.4 of σ or $\sim 10 \text{ km s}^{-1}$. Rotation velocities can be detected down to $\sim 5 \text{ km s}^{-1}$, if present.

3. SAMPLE SELECTION

We chose a sample of galaxies that span a wide range in redshift, stellar mass, and morphology. The DEEP2 survey had magnitude limits of $R_{AB} = 24.1$, bright enough to yield good HST/ACS imaging. A redshift limit of $z = 1.2$ ensures that galaxies of all colors on the “blue sequence” (Willmer et al. 2006) are well-sampled. To yield good quality kinematics, emission lines were required to have integrated intensities $> 1500 \text{ e}^-/\text{\AA}$ in the summed one-dimensional spectrum, and spectrographic slits had to be aligned to within 40° of the major axes of the galaxies (see Fig. 13 of Weiner et al. 2006a). Also, to

reduce the effects of dust, edge-on systems with $i > 70$ were excluded, and to allow a reliable rotation measure, nearly face on galaxies with $i < 30$ were removed. A total of 14 galaxies were excluded because they had emission lines with disturbed morphologies or that had contamination by emission from a nearby galaxy on the sky. After additional cosmetic cuts were made (Kassin et al. in preparation), the final sample became 544 galaxies. Our final sample is primarily selected on emission line strength.

4. DATA REDUCTION AND ANALYSIS

4.1. Photometric Parameters

In order to interpret dynamical measurements made from the spectra, accurate position angles and ellipticities of galaxies must be obtained from HST imaging. To measure these parameters, the SExtractor galaxy photometry software (Bertin & Arnouts 1996) is used, as discussed in Lotz et al. (2006). To obtain quantitative morphologies for galaxies, we use the Gini/ M_{20} method of Lotz, Primack, & Madau (2004). This system of objective structural parameters has been shown to reliably divide galaxies into bins analogous to Hubble types; namely, early type spirals, late type spirals and irregulars, and major mergers. Galaxies are classified in the V image for $z < 0.6$ and in I for $z \geq 0.6$. Such quantitative morphologies are obtainable only for galaxies with Petrosian radii $> 0.3''$, images that have a signal-to-noise ratio of > 2.5 , and that do not fall near the edge of the HST/ACS CCD chip. Galaxies without quantitative morphologies are not removed from the sample for completeness sake, and do not differ statistically from the rest of the sample. All photometric parameters, including quantitative morphologies, will appear in a forthcoming paper, Lotz et al. (2007). In a separate exercise, we visually classified all galaxies and found examples that were fairly normal according to Gini/ M_{20} , but looked to our eye to be more disturbed or compact; we discuss these galaxies separately.

4.2. Spectroscopic Measurements

Spatially extended emission lines in the galaxy spectra are used to measure gas rotation and dispersion profiles. Since the spatial extent of the line emission is at most only a few times the seeing (typically $0.7''$ FWHM), the effect of seeing must be modeled. We do this with the ROTCURVE fitting procedure of Weiner et al. (2006a). The kinematic model we fit has two parameters: the velocity on the flat part of the rotation velocity profile, V_{rot} , and the velocity dispersion from a spatially resolved fit to the two-dimensional spectra, σ_g . The best-fit V_{rot} values are corrected for inclination with the measured galaxy ellipticities. For galaxies without a disk-like geometry (based on visual inspection of HST/ACS images), V_{rot} is not inclination-corrected. These galaxies are flagged in the following analysis, but fits do not change if all galaxies are inclination-corrected. The σ_g we measure does not have to correspond to a literal gas velocity dispersion like that of stars in an elliptical galaxy. Instead, for $\sigma_g \lesssim 20 \text{ km s}^{-1}$, σ_g likely measures the relative motions of individual H II regions, as in spiral arms or a thick disk; for $\sigma_g \gtrsim 20 \text{ km s}^{-1}$, σ_g likely represents an effective velocity dispersion caused by the blurring of velocity

gradients on scales at or below the seeing limit that may not even have a preferred plane. An uncertainty of 0.1 dex is adopted in both σ_g and the inclination-corrected V_{rot} to account for random errors and the dependence of the model parameters on the assumed seeing and scale radius of the rotation curve. Results do not change significantly if uncertainties of 0.2 are chosen, as discussed in §6.

5. STELLAR MASS ESTIMATES

A few methods of estimating the stellar masses (M_*) of galaxies have been investigated in a separate study (Kassin et al. in preparation). These methods are: a color- M/L relation from Bell et al. (2003) for $B - V$ and M/L_B , a color- M/L relation from Bell et al. (2003) for $B - V$ and M/L_H , $M/L_H = 1$, broad-band spectral energy distribution (SED) fits of Bundy, Ellis, & Conselice (2005) which incorporate observed optical and K -band data, and the method of Lin et al. (2006). We choose to adopt the method of Lin et al. (2006). These authors calibrated rest-frame UBV photometry and redshifts to the full SED fits of Bundy et al. (2005) to obtain M_* estimates for very blue galaxies that are not detected at K , which Bundy et al. (2005) require to derive a M_* . While the evolution of SEDs with redshift is included and errors of 0.2 dex are assumed, the results of this paper, as discussed next, change insignificantly if we do not take into account evolution or increase the errors to 0.3 dex (Kannappan & Gawiser 2007).

6. $S_{0.5}$ AS A TRACER OF GALAXY-DARK HALO POTENTIAL WELLS

The quantity $S_K^2 \equiv KV_{rot}^2 + \sigma_g^2$, where K is a constant, combines dynamical support from ordered motion with that from disordered motions (Weiner et al. 2006a). For a spherically symmetric tracer population with isotropic velocity dispersion and density $\propto r^{-\alpha}$, $\sigma_g = V_{rot}/\sqrt{\alpha}$ (Binney & Tremaine 1987, §4.4), where $K \equiv 1/\alpha$. Therefore, if galaxies are virialized systems, and these assumptions about the tracer population are at least approximately correct, then S_K should at least approximately trace the global σ of galaxy-halo systems. In this case, the tracer population is the gas producing the emission lines, which we assume follows the M_* . For disk galaxies with exponential M_* profiles, $\alpha \simeq 2 - 3$ brackets a range of reasonable values (§5.2 of Weiner et al. 2006a). A satisfactory approximation is adopted for all morphologies, $K = \frac{1}{2}$; if $K = \frac{1}{3}$ is adopted, the overall results do not change. We henceforth use $S_{0.5}$ for our analysis.

7. RESULTS

The top panel of Figure 1 shows V_{rot} versus M_* (the V_{rot}/M_* TFR) for a range of redshifts. The majority of spirals (green triangles and blue squares not outlined in black) form a clear ridge-line that compares well to a local relation from Bell & de Jong (2001), consisting of well-ordered spirals, and to a $z \sim 1$ relation from Conselice et al. (2005), who included only “elongated disks.” In contrast, almost all of the other classes (red circles and symbols outlined in black) lie to lower V_{rot} , causing a large scatter (~ 1.5 dex in velocity).

This morphological dependence of Tully-Fisher scatter is well known. Among local studies, e.g., larger

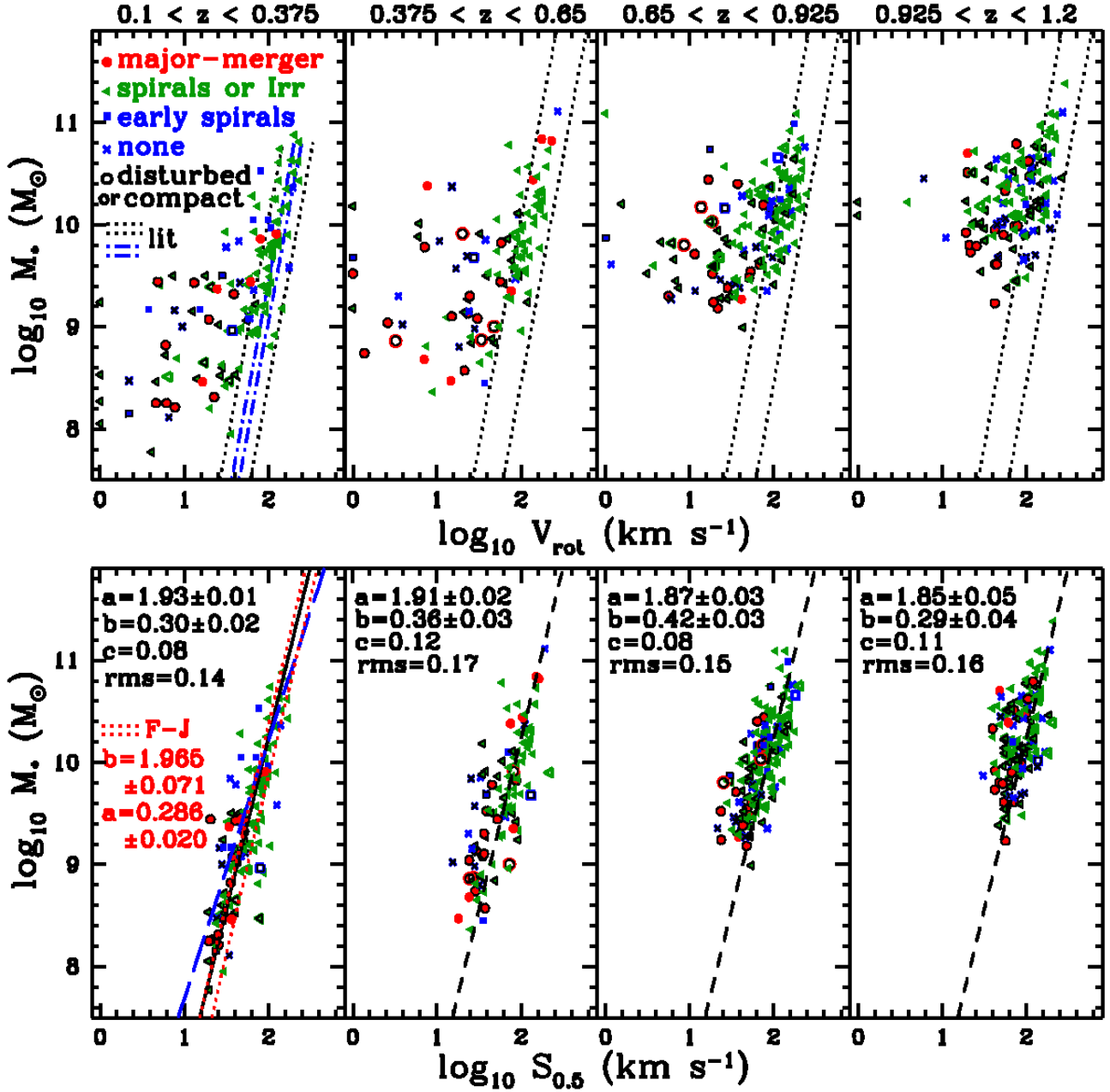


FIG. 1.— The $S_{0.5}$ and V_{rot} stellar-mass Tully-Fisher relations (M_* TFRs) for $0.1 < z < 1.2$ in bins of z . Galaxies are plotted as different symbols according to their quantitative morphologies, and if a morphology is unobtainable, it is placed into the ‘none’ category. Symbols are outlined in black if the galaxies were considered to be disturbed or compact via a separate visual classification. If V_{rot} is not inclination corrected, open symbols are used; all galaxies in the ‘none’ category are inclination-corrected as their symbol does not have an open form. Using $S_{0.5}$, which combines the dynamical support from ordered motion with that from disordered motions, results in an M_* TFR that is much tighter and non-evolving to $z = 1.2$. For $S_{0.5}$, a fit to data in the lowest z bin is plotted as a solid line that is repeated in the other z bins as dashed lines. Fits are labeled in each box, where a is the intercept at $10^{10} M_\odot$, b the slope, c the intrinsic scatter in $S_{0.5}$, and rms the rms scatter in $S_{0.5}$. In the lowest z bin for V_{rot} , the M_* TFRs from local and $z \sim 1$ studies (Bell & de Jong 2001 and Conselice et al. 2005, respectively) are plotted as two dot-dashed and dotted lines, respectively, to delineate rms scatter. In the lowest z bin for $S_{0.5}$, the local M_* Faber-Jackson relation (Gallazzi et al. 2006) is plotted as two dotted lines to delineate rms scatter. All relations from the literature have been converted to a Chabrier initial mass function when necessary. An estimate of the $S_{0.5}/M_{\text{baryon}}$ TFR (§9) is plotted as a long dashed blue line in the lowest z bin.

scatter is found for close pairs with kinematic disorders (Barton et al. 2001) and when peculiar galaxies are included (Kannappan et al. 2002). At higher redshifts, larger scatter is found for $z \sim 0.5$ galaxies with “complex kinematics” (Flores et al. 2006). Moreover, $\sim 25\%$ of galaxies found with kinematics unrelated to rotation are excluded from Tully-Fisher studies at $0.25 < z < 0.45$ (Simard & Pritchett 1998) and at $0.1 < z < 1.0$ (Böhm et al. 2004). In summary, because of morphological pruning, no study except that of Weiner et al. (2006b) incorporates the population of Tully-Fisher outliers that we detect in a measurement of Tully-Fisher evolution, and the conclusions of such studies will only apply for the subsample of galaxies that are morphologically well-ordered.

For $M_* > 10^{10} M_\odot$, the percentage of galaxies that scatter to low V_{rot} from the Tully-Fisher ridge-line (defined as the left-most dotted line in Figure 1) increases with redshift (18%, 35%, 42%, and 62% for the four redshift bins plotted). Similarly, Weiner et al. (2006a) find bright galaxies with $\sigma_g > V_{rot}$ at $z \geq 0.5$ that are rare at low redshift.

The bottom panel of Fig. 1 uses $S_{0.5}$ instead of V_{rot} in the M_* TFR. The resulting relation has scatter that is not much greater than our measurement uncertainties and does not evolve significantly with z .⁸ Evidently, galaxies with low V_{rot} compared to the V_{rot}/M_* TFR ridge-line have a significant σ_g component which causes them to lie on the $S_{0.5}/M_*$ TFR. Lines are fit to the $S_{0.5}/M_*$ TFR in the four redshift bins in Fig. 1 with a maximum likelihood method detailed in Weiner et al. (2006b). We fit $\log_{10} S_{0.5} = a + b \log_{10} M_*$ and all excess scatter is allocated to the $S_{0.5}$ -coordinate. The fits do not vary significantly for the different redshift bins. Average values for the slope, intercept at $10^{10} M_\odot$, and intrinsic scatter over all redshifts are 0.34 ± 0.05 , 1.89 ± 0.03 , and 0.10 dex in $S_{0.5}$. The average rms scatter is 0.16 dex in $S_{0.5}$, which corresponds to 0.47 dex in M_* (~ 1.2 magnitudes). The fitted relations are not very sensitive to the error estimates for $S_{0.5}$ and M_* ; changing either error estimate by ± 0.1 dex changes fit intercepts within the $1-\sigma$ error, and slopes by not more than ± 0.1 dex. However, our limited M_* range at higher redshift makes slope measurements more uncertain than the formal fit errors. Furthermore, different estimates of M_* can yield a range of ~ 0.2 dex in intercept, and M_* estimators with non-evolving SEDs can cause the $S_{0.5}/M_*$ TFR to show ~ 0.1 dex evolution in intercept with redshift, but this reflects problems of these estimators rather than actual evolution in the $S_{0.5}/M_*$ TFR.

Since no Tully-Fisher sample at low or high redshift has as much scatter as our V_{rot}/M_* TFR due to morphological pruning, it is rather remarkable that the $S_{0.5}/M_*$ TFR scatter for the same sample of galaxies manages to approach as close as it does to the scatters found for the V_{rot}/M_* TFRs for galaxies with relatively undisturbed

⁸ One would expect a small (~ 0.05 dex) decrease in intercept from $z = 1$ to $z = 0$ due simply to the predicted increase in M_* of $\sim 50\%$ for a typical spiral galaxy ($z_{formation} = 5$ and an exponentially decreasing star formation rate with $\tau = 7$ Gyr), but it would not be detectable given our errors. We do not attempt to determine K by minimizing the scatter in the S_K/M_* TFR because K is sensitive to the morphological mix of the sample and the distribution of measurement errors.

morphologies (~ 0.6 dex in M_* for Conselice et al. 2005). In addition, Fig. 1 shows that the M_* Faber-Jackson relation for low redshift ($0.005 < z \leq 0.22$) early type galaxies from Gallazzi et al. (2006) is consistent with the $S_{0.5}/M_*$ TFR in terms of slope and intercept.

8. DISCUSSION

If those galaxies with $M_* > 10^{10} M_\odot$ that are off the V_{rot}/M_* TFR ridge-line with low V_{rot} at higher redshift eventually form into well-ordered disk galaxies on the ridge-line, this trend implies that more massive disk galaxies may be moving onto the V_{rot}/M_* TFR with time as their stars and gas “settle” into more circular/planar-dominated orbits. The possible mechanisms behind this settling can be circularization of gas orbits, gaseous dissipation to the disk plane, and/or mergers ending with the growth of a gaseous disk. The scatter for $M_* \leq 10^{10} M_\odot$, which we can observe at lower redshift, is also large, suggesting that lower M_* galaxies may currently be settling.

A scenario of galaxy formation that is consistent with our results is one that begins with matter assembling in dark halo potential wells with random orbital kinematics. The baryonic components form proto-disks that are initially supported by a combination of ordered and random motions. The material in these proto-disks has been settling since then, unless they undergo major mergers. Over the last half or so of their lives, proto-disks and their descendants lie on nearly the same $S_{0.5}/M_*$ TFR. At first glance, the similarity between the Faber-Jackson relation and the $S_{0.5}/M_*$ TFR in slope and intercept is reassuring, given that merging proto-disks on parabolic binary orbits should put the merger products close to the Faber-Jackson relation in Fig. 1 (e.g., Robertson et al. 2006). This suggests that the origin of the Faber-Jackson relation could in fact be the pre-existing $S_{0.5}/M_*$ TFR for disk-like galaxies, if merging is the process that creates ellipticals. However, additional studies are needed to confirm this speculative scenario.

9. RELATION TO HALO KINEMATICS

If the framework we adopt is correct, halo kinematic properties should be related to measurable galaxy kinematics. In particular, N-body models show that the slope of the relation between halo mass (M_s) and halo σ (σ_s), both measured within the scale radius (Navarro, Frenk, & White 1997), is 0.33: $\log_{10} \sigma_s = 0.33 \log_{10} M_s + \text{constant}$. Remarkably, this slope is nearly consistent with both galaxy relations. In addition, neither the halo $\sigma_s - M_s$ relation, nor M_s or σ_s individually, is predicted to evolve to within $\sim 10\%$ from $z = 1.2$ to now (Diemand et al. 2007; see Wechsler et al. 2002 for evolution in terms of virial quantities). So, if $S_{0.5}$ is linearly related to halo σ_s and $M_*/M_s = \text{constant}$, then the $S_{0.5}/M_*$ TFR should also evolve little from $z = 1.2$, in agreement with observations. Furthermore, that neither M_s nor σ_s individually evolves might imply that absolute changes in inner baryon structures are also small.

However, when comparing galaxies to halos, there are at least three major complications. First, since M_* is subject to the star-formation history of a galaxy, it is not as fundamental a quantity as baryonic mass (M_{baryon}). Locally, low- M_* galaxies have a greater gas-to-star fraction than more massive galaxies (e.g., McGaugh 2005), so the low-redshift $S_{0.5}/M_{baryon}$ TFR ought to have a

steeper slope than the $S_{0.5}/M_*$ TFR. Indeed, if we assume that $M_{\text{gas}} = 0.56M_* + 3.96$ (roughly consistent with data from McGaugh 2005 using relations from Bell et al. 2003 to obtain M_* , which we later convert to a Chabrier 2003 initial mass function), then the $S_{0.5}/M_*$ TFR slope in the lowest redshift bin steepens to ~ 0.39 . Secondly, galaxies should convert gas into stars over time, causing evolution in M_*/M_s . The third issue is the complicated relation between $S_{0.5}$ and σ_s , which is expected to be affected by baryon dissipation and the response of the dark halo to it (e.g., Blumenthal et al. 1986), neither of which are completely understood. With a better understanding or measurement of these factors and their time evolution, the relationship between galaxy and halo scal-

ing laws will ultimately become clearer and the effects of baryonic processes during galaxy formation may even be elucidated.

We acknowledge the following grants: NSF AST-0507483, HST GO-10134, and HST AR-09936 and the very significant cultural role and reverence that the summit of Mauna Kea has always had within the indigenous Hawaiian community and appreciate the opportunity to conduct observations from this mountain. SAK would like to thank A. Faltenbacher, B. Holden, and Z. Zheng for helpful conversations.

REFERENCES

Barton, E. J. et al. 2001, AJ, 121, 625
 Bell, E. F. & de Jong, R. S. 2001, ApJ, 550, 212
 Bell, E. F., McIntosh, D. H., Katz, N., & Weinberg, M. D. 2003, ApJS, 149, 289
 Bertin, E. & Arnouts, S. 1996, A&A, 117, 393
 Binney, J. & Tremaine, S. 1987, Galactic Dynamics (Princeton: Princeton Univ. Press)
 Blumenthal, G. R., Faber, S. M., Flores, R., & Primack, J. R. 1986, ApJ, 301, 27
 Böhm, A. 2004, A&A, 420, 97
 Bundy, K., Ellis, R. S., & Conselice, C. J. 2005, ApJ, 625, 621
 Chabrier, G. 2003, PASP, 115, 763
 Conselice, C. J., et al. 2005, ApJ, 628, 160
 Dalcanton, J. J., Spergel, D. N., & Summers, F. J. 1997, ApJ, 482, 659
 Davis, M., et al. 2006, ApJ, accepted, astro-ph/0607355
 Davis, M., et al. 2003, Proc. SPIE, 4834, 161
 Diemand, J., et al. 2007, in preparation
 Flores, H., et al. 2006, A&A, 455, 107
 Gallazzi, A., Charlot, S., Brinchmann, J., & White, S. D. M. 2006, MNRAS, 370, 1106
 Kannappan, S., Fabricant, D. G., & Franx, M. 2002, ApJ, 123, 2358
 Kannappan, S. J. & Gawiser, E. 2007, ApJ, accepted, astro-ph/0701749
 Kassin, S. A., et al., in preparation
 Lin, L., et al. 2006, ApJ, accepted, astro-ph/0607272
 Lotz, J. M., Primack, J., & Madau, P. 2004, AJ, 128, 163
 Lotz, J. M., et al. 2006, astro-ph/0602088
 Lotz, J. M., et al. 2007, in preparation
 McGaugh, S. S. 2005, ApJ, 632, 859
 Navarro, J. F., Frenk, C. S., & White, S. D. M. 1997, ApJ, 490, 493
 Pizagno, J. et al., 2005, ApJ, 633, 844
 Robertson, B. et al. 2006, ApJ, 645, 986
 Simard, L. & Pritchett, C. J. 1998, ApJ, 505, 96
 Wechsler, R. H. et al. 2002, ApJ, 568, 52
 Weiner, B. J., et al. 2006a, ApJ, 653, 1027
 Weiner, B. J., et al. 2006b, ApJ, 653, 1049
 Willmer, C. N. A. 2006, ApJ, 647, 853